7-2020

Parametric study of a triboelectric transducer in total knee replacement application

Alwathiqbellah Ibrahim
University of Texas at Tyler

Geofrey Yamomo
The University of Western Ontario

Ryan Willing
The University of Western Ontario

Shahrzad Towfighian
Binghamton University--SUNY, stowfigh@binghamton.edu

Parametric Study of a Triboelectric Transducer in Total Knee Replacement Application

Journal Title
XX(X):2–21

DOI: 10.1177/ToBeAssigned
www.sagepub.com/
SAGE

Alwathiqbellah Ibrahim [1], Geofrey Yamomo [2], Ryan Willing [2], and Shahrzad Towfighian[3]

Abstract

Triboelectric energy harvesting is a relatively new technology showing promise for biomedical applications. This study investigates a triboelectric energy transducer for potential applications in total knee replacement (TKR) both as an energy harvester and a sensor. The sensor can be used to monitor loads at the knee joint. The proposed transducer generates an electrical signal that is directly related to the periodic mechanical load from walking. The proportionality between the generated electrical signal and the load transferred to the knee enables triboelectric transducers to be used as self-powered active load sensors. We analyzed the performance of a triboelectric transducer when subjected to simulated gait loading on a joint motion simulator. Two different designs were evaluated, one made of Titanium on Aluminum, (Ti-PDMS-Al), and the other made of Titanium on Titanium, (Ti-PDMS-Ti). The Ti-PDMS-Ti design generates more power than Ti-PDMS-Al and was used to optimize the structural parameters. Our analysis found these optimal parameters for the Ti-PDMS-Ti design: external resistance of $304\ M\Omega$, a gap of $550\ \mu m$, and a thickness of the triboelectric layer of $50\ \mu m$. Those parameters were optimized by varying resistance, gap, and the thickness while measuring the power outputs. Using the optimized parameters, the transducer was tested under different axial loads to check the viability of the harvester to act as a self-powered load sensor to estimate the knee loads. The forces transmitted across the knee joint during activities of daily living can be directly measured and used for self-powering, which can lead to improving the total knee implant functions.

Keywords

Triboelectric harvester, Energy Harvesting, TKR, Gait loading.

Prepared using sagej.cls *[Version: 2017/01/17 v1.20]*

Introduction

The high demand for portable and wireless sensor networks has inspired the development of robust and independent energy harvesting mechanisms to eliminate the need for batteries (Roundy et al. (2003)). With increasing interest in the biomedical sector for self-powered sensors (Tang et al. (2015); Stellbrink and Trappe (2007)), harvesting energy from natural human motions is an attractive concept. Human motion can be a ubiquitous energy source to power autonomous sensors embedded in orthopedic implants, where the electrical charge harvested can be used to power telemetry systems for measuring joint loads. The concept of self-powered sensors eliminates the need for wires or depleting power sources like batteries; enabling long-term measurement applications inside the human body. Activities of Daily Living (ADLs) transfer a wide range of loads through human joints. The knee joint is the largest in the human body and sustains substantial stresses exceeding several times body weight (BONNER (2007)). After joint replacement surgeries, such as total knee replacement (TKR), implanted components must sustain these loads for decades without excessive wearing, deformation or fatigue. Unfortunately, aberrant loading patterns resulting from implant misalignment, imbalance or loosening may subject these components to loads for which they were not designed, accelerating damage progression and often requiring revision. Thus, the ability to measure loads transmitted through TKRs using embedded autonomous sensors can enable earlier identification of aberrant loading and provide an opportunity for interventions that may correct the issue and extend the longevity of the implant, avoiding costly and risky revision surgeries (Ong et al. (2010)). Previous works for intra-operative sensors have focused on the mechanical behavior of the knee joint and quantification of the load transferred through TKR components (Meneghini et al. (2016); Gustke et al. (2014); Roche et al. (2014)), however, the applications of such systems are limited to the operating room. Instrumented components have been used initially by D'Lima's group (D'Lima et al. (2005); D'Lima et al. (2006); D'Lima et al. (2007)) and Bergmann's group (Kutzner et al. (2010, 2011)), however, they are mostly limited to the lab. The stem and keel of these components were hollowed out to house signal conditioners, microprocessors, and telemetry (D'Lima et al. (2005)). Load imbalances are important to measure in TKR. The accurate measurement of these loads can help to determine the wear in polyethylene, stress distribution in the implant and the implant-bone interface, and the stress transferred to the underlying bone (Kaufman et al. (1996)).

To make self-powered load monitoring, piezoelectric and electromagnetic mechanisms have been the subject of research for TKR applications (Platt et al. (2005); Almouahed et al. (2013); Luciano et al. (2012)). The work completed by Platt et al. (2005) shows that the piezoelectric mechanism is promising

[1] University of Texas at Tyler, 3900 University Blvd, Tyler, TX 75799, USA.
[2] University of Western Ontario, London, ON N6A 3K7, Canada.
[3] Binghamton University, 4400 Vestal Parkway E., Binghamton, NY 13902, USA.

Corresponding author:
Shahrzad Towfighian, Binghamton University, 4400 Vestal Parkway E., Binghamton, NY 13902.
Email: stowfigh@binghamton.edu

Prepared using sagej.cls

for load sensing in TKR applications. Knee loads were detected under walking activity using four piezoelectric transducers placed between the tibial tray and a polyethylene bearing (Almouahed et al. (2013)). In a recent study, Safaei et al. (2018) presented an optimized design prototype by embedding the piezoelectric sensor in the polyethylene bearing to meet FDA standards. However, piezoelectric ceramics are brittle and may not endure high loads at the knee joint. The electromagnetic generators designed by Luciano et al. (2012) are complicated and may not be easily incorporated into a variety of implant designs because they are difficult to fit in the knee and require coils to operate.

One of the most recent transducers, the triboelectric mechanism, is based on the coupling of contact electrification and electrostatic induction that is used for both energy harvesting and sensing (McCarty and Whitesides (2008); Baytekin et al. (2011)). This mechanism was found to be a promising technology because of many advantages such as high output power, flexibility, environmental friendliness, biocompatibility, low-cost materials, and simple fabrication (Fan et al. (2012); Zhu et al. (2013); Wang et al. (2013); Hu et al. (2013)). When two materials; with different tendencies to lose and gain electrons, come into contact with each other, the two materials become electrically charged based on the conjunction of triboelectrification and electrostatic induction mechanisms (Zi et al. (2016); Wang (2015); Yi et al. (2015); Zhou et al. (2014); Zeng et al. (2013); Zhang et al. (2014)). The triboelectric mechanism has been used recently to harvest energy from a variety of sources, such as human walking (Wang et al. (2014b); Ibrahim et al. (2019)), mechanical vibration (Ibrahim et al. (2018)), rotation (Han et al. (2014)), and other applications (Bae et al. (2014); Su et al. (2014); Farhangdoust et al. (2019)). Because of a direct relationship between the mechanical load and surface charge density (Jin et al. (2016); Hossain et al. (2020)), which governs electrical output, this mechanism can be used as a self-powered sensor (Lin et al. (2013); Zhang et al. (2013); Lin et al. (2014)). In our previous work (Ibrahim et al. (2019)), we reported a feasibility study for a TKR load sensor application based on a triboelectric transducer. The generated power via this phenomenon was estimated to be sufficient to power a digitizing circuit (Jain et al. (2019)). More in-depth analysis is needed to characterize triboelectric transducers for specific sensing applications and broaden their commercial use.

Material and structural properties have a considerable influence on the performance of triboelectric transducers. Materials with greater tendencies to lose electrons contacting other materials that have more tendency to gain electrons increases output power (Gomes et al. (2018); Gooding and Kaufman (2011); Burgo et al. (2016)), and these tendencies can be referenced from the Triboelectric Polarity Series. Structural parameters also affect output and can be optimized to maximize the energy harvested. Furthermore, energy harvested could be maximized by estimating the optimum resistance and load capacitance (Niu et al. (2015)). This optimum load capacitance is found to be linearly proportional to the numbers of the charging cycle and the inherent capacitance for the triboelectric harvester. Because of the effects, structural material and electrical properties have on the performance of these harvesters, more in-depth analysis is required to make these harvesters suitable for $in\ vivo$ applications. In our previous study of triboelectric generators for TKR applications (Ibrahim et al. (2019)), we did not report the parameters that can have a significant effect on the output of the triboelectric generators. Therefore, in this article, we mainly focus on the geometrical and system parameters to extract the maximum power for this specific application and evaluate the transducer performance for load sensing. To assess the sensitivity to walking activities, we include analysis for the triboelectric transducer under a simulated

walking gait using AMTI VIVO Simulator.

In the construction of triboelectric energy transducers, it is very important to take into consideration the main parameters that can enhance the performance. Particularly, selecting proper materials and geometry such as internal resistance, the insulator thickness, and the gap space between the harvester layers can play a significant role in the output. This paper investigates the effect of these parameters on the self-powered mechanism for TKR applications. Two different designs are compared; both featuring a Titanium-on-Polydimethylsiloxane (Ti-PDMS) contact interface, but different materials for the electrostatically charged electrode underlying the PDMS layer (Titanium or Aluminum; Ti-PDMS-Ti or Ti-PDMS-Al). The paper is divided to two main sections: AMTI VIVO Simulator Analysis, where we test and analyze mainly the Ti-PDMS-Al harvester and the Parametric Study, where we evaluate the effect of system parameters on Ti-PDMS-Ti harvester. In the first section, the performance of triboelectric energy harvesters subjected to simulated walking gait (walking) loading on a joint motion simulator is characterized. The results obtained from the VIVO simulator found to be promising and showed the Ti-PDMS-Ti has a larger output compared to the Ti-PDMS-Al harvester. Thus, in the second section, to perform the parametric study, the Ti-PDMS-Ti harvester was tested under a Material Testing System (MTS) to evaluate the effect of electromechanical parameters. The reason for switching to the MTS machine in the second section, was the lack of the VIVO simulator at Binghamton University (USA) and traveling complications to the University of Western Ontario (Canada) where the VIVO simulator was located. To maintain accuracy, we conducted testing at physiologically relevant loading magnitudes.

AMTI VIVO Simulator Analysis

Triboelectric Harvester Configuration and Assembly

A schematic for the triboelectric harvester configuration is illustrated in Fig. 1a. The harvester is made of two layers, an upper Ti and a lower polydimethylsiloxane (PDMS) insulator bonded to another Ti layer to create (Ti-PDMS-Ti) harvester or an Al layer to create (Ti-PDMS-Al) harvester. The upper Ti and lower PDMS layers have reverse micro-patterned surfaces (sawtooth ridges). PDMS is a commonly used polymer, because of its flexibility, manufacturing ease, transparency, biocompatibility, and super-hydrophobicity. It is also widely used as triboelectric material in the construction of triboelectric harvesters for a broad range of applications (Zhu et al. (2016); Ko et al. (2014); Zheng et al. (2016)). On the other hand, Ti has suitable mechanical properties for this application (strength and stiffness), and it is a biocompatible material. A rubber spring is located at each of the four corners, and the springs separate the two layers.

A simulated gait load is used to test the performance of the triboelectric harvesters. The simulated gait load is produced by an AMTI VIVO joint motion simulator. The triboelectric harvester operates based on contact electrification and electrostatic induction. When a cyclic compressive load is applied to the harvester, the mechanical rubber springs will be compressed to allow the upper and lower layers to periodically contact each other, which creates an alternating current. For more information about the working mechanism of triboelectric harvesters, readers can refer to Fan et al. (2012). Two identical harvesters are centered at the medial and lateral positions between the tibial tray and UHMWPE bearing as shown in Fig. 1b. Under the applied gait, the harvesters on medial and lateral parts will receive different

loads and the difference is indicated by a voltage difference between them. To minimize stress and allow only vertical motion, we use four guide bolts to connect the tibial tray and the bearing. For practical applications, these triboelectric harvesters will be placed inside a package that will be designed to yield the required contact and separation under applied loads and the rubber springs will be removed.

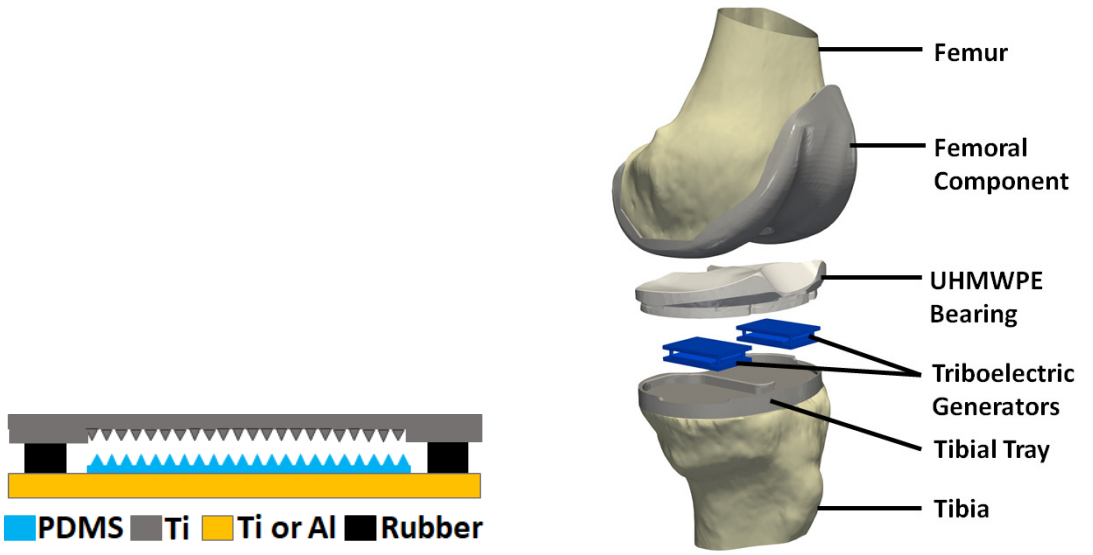

(a) **(b)**

Figure 1. (a) Schematic of the triboelctric energy harvester. (b) 3D model of the instrumented knee implants simulator

Experimental Setup

The experimental setup used to examine the harvester performance comprises a simulator control unit, the AMTI VIVO joint simulator, a Keithley 6514 electrometer, and an ExceLINX4 (Fig. 2). The control unit and the AMTI VIVO simulator are used to create the simulated gait load and transfer it to the harvesters, while the electrometer is used to measure voltage and current signals generated by the harvesters. The applied load force only included the vertical compressive load because this component is the most significant among other components. Both harvesters were tested with the simulator. The upper Ti layer in the Ti-PDMS-Al harvester is *3D* printed using ProX DMP 320 printer and (Fig. 3a), while the upper Ti layer in the Ti-PDMS-Ti harvester was *CNC* machined (Fig. 3b). The *CNC* machined mold had a better resolution in creating micropatterns, so it was used to make the second prototype. The Ti-PDMS-Al harvester measured approximately *30 x 15 x 3 mm* and was made of a *1 mm* thick 3D printed Ti plate with sawtooth micropattern (300 tooth height) and a matching sawtooth pattern on a mating PDMS layer. The PDMS layer adhered to another 1 mm thick Al layer. Ti-PDMS-Ti triboelectric harvester measured approximately *30 x 15 x 2 mm* with similar sawtooth wavelength, but the micropatterned metal layer was

made of $0.5\ mm$ thick Ti. There is a minor difference in micro-patterns as the *CNC* machined features are dull compared to sharp features of the 3D printed prototype. We hypothesize the small variation in the shape of the micro-patterns does not have a considerable effect on the output as the wavelength does (Dhakar et al. (2014)). The microscopic images for the mold micropattern, PDMS with reverse micropattern, and the lower layers for both triboelectric harvesters are shown in Fig. 3.

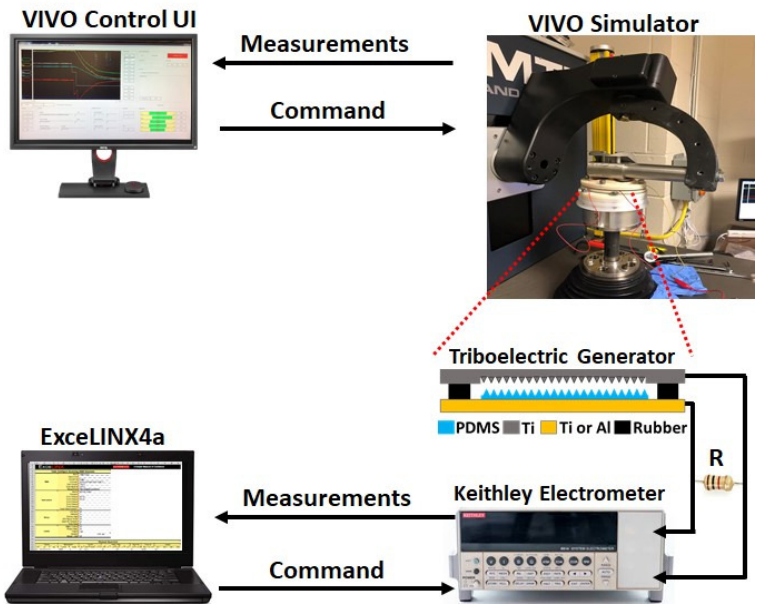

Figure 2. The experimental setup used to test the triboelectric harvesters using AMTI VIVO simulator.

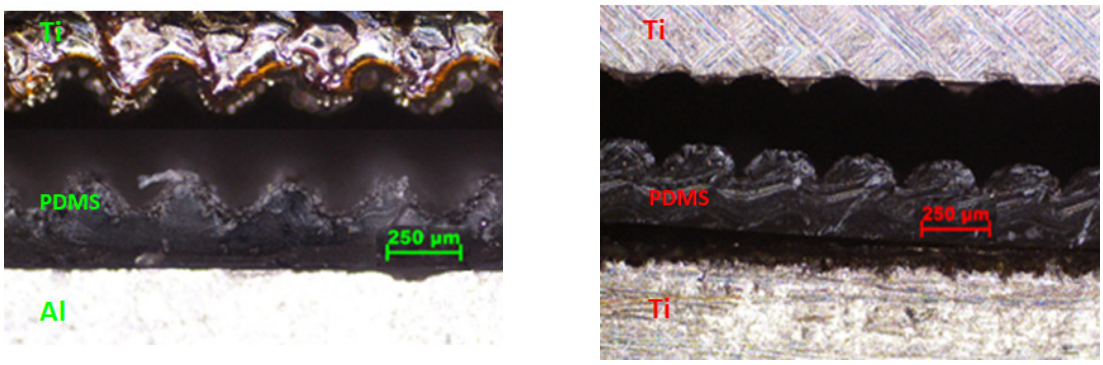

(a) **(b)**

Figure 3. Microscopic images for the triboelectric harvesters (a) Ti-PDMS-Al. (b) Ti-PDMS-Ti. The upper Ti layer looks different because in (a) the Ti layer is $3D$ printed, while in (b) it is CNC machined.

Results and Discussions

During gait, the maximum vertical (compression) force transmitted through the knee exceeds 2000 N. Initially, the prototypes were tested at full gait compressive load (2000 N) adopted from Bergmann et al. (2014), and a failure in the rubber spring occurred. To overcome this issue, we decided to scale-down the vertically applied compression force to 800 N instead of the full gait load (2000 N), however, a physiological loading pattern with respect to time, Bergmann et al. (2014), was maintained (Fig. 4a). Next, to understand the response behavior of the triboelectric energy harvesters under an applied gait load, the Ti-PDMS-Al harvester is tested at *800 N* and generated a maximum peak voltage of 10 V as shown in Fig. 4b. Comparing the plots in Fig. 4, we can notice that the timescales were not synchronized and the main reason for this is that two independent instruments were used to measure the load gait and the voltage. The gait load is measured using a built-in load cell in the VIVO simulator, while the voltage is measured using a Keithley electrometer. The measured zoomed-in and overlapped gait profile and the corresponding voltage-time response are shown in Fig. 5. Both profiles have three distinct regions; S: Separation, A: Approaching, C: Contact with respect to the motion of the VIVO simulator. At some point after contact, the triboelectric harvester layers start to separate and reach the minimum gait load when full separation occurs; as the layers separate, the corresponding generated voltage starts to increase rapidly to reach its maximum value, region S in Fig. 5. Region C in this figure shows when the voltage drops to zero at the contact, the triboelectric and electrostatic charges stabilize. The behavior in the region A, when two layers approach, is more complicated and can be explained by having a closer look at an electrical model for the harvester. The electrical model of the harvester consists of a voltage source in series with a variable capacitor and an internal resistance. The voltage generated by the harvester and measured across an external resistance, R is governed by Eq. (1) (Ibrahim et al. (2019))

$$V(t) = R\frac{dQ}{dt} = -\frac{Q(t)}{S\epsilon_0}\left(\frac{t_0}{\epsilon_r} + d_0 - x(t)\right) + \frac{\sigma(d_0 - x(t))}{\epsilon_0} - r\frac{dQ}{dt} \tag{1}$$

where on the right, the first term represents the voltage potential difference due to transferred charges, the second term indicates the voltage potential difference from the triboelectric charges between two conductors, and the third term shows the voltage drop across the internal resistance, r. In Eq. (1), t_0 represents the PDMS thickness, d_0 is the initial gap, S is the generator area, Q is the induced charge, ϵ_0 is the dielectric constant of air, ϵ_r is the dielectric constant of PDMS, $d_0 - x(t)$ is the varying gap, and σ is the triboelectric charge density on the surface of the PDMS. The variation of the force changes the gap between the two harvester layers ($d_0 - x(t)$) as well as σ. The sign of the voltage across external resistance R (the left-hand side of this equation) depends on whether the positive term or negative terms will have a larger magnitude.

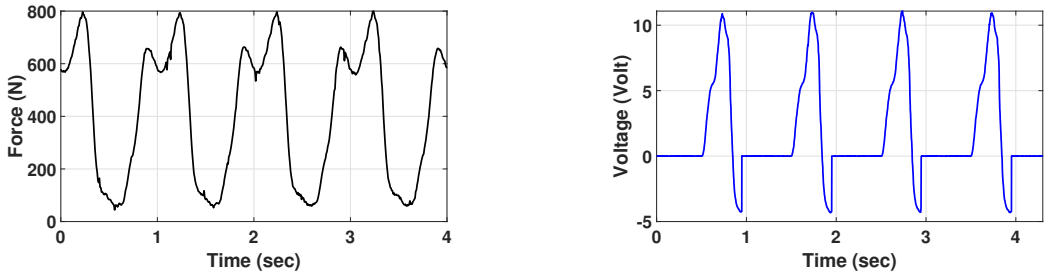

(a) **(b)**

Figure 4. (a) Load profile for a knee partial gait load simulated by AMTI VIVO joint motion simulator. (b) Generated output voltage signal.

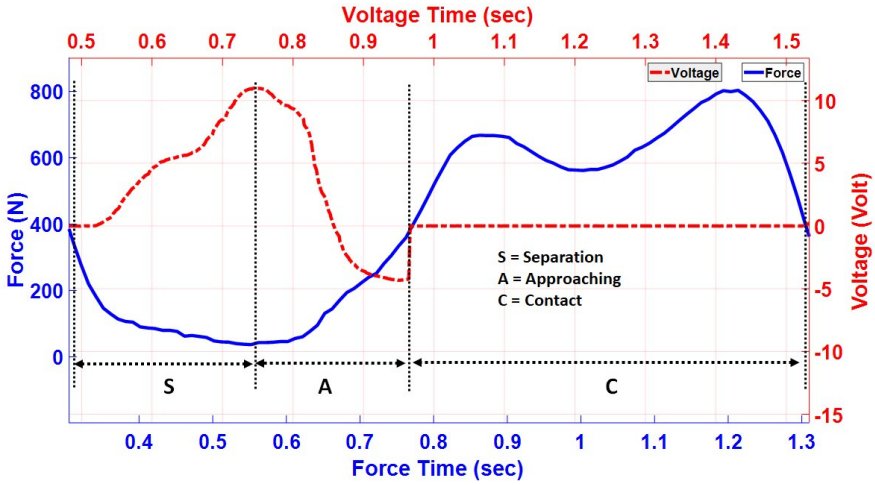

Figure 5. Zoomed-in and overlapped signals of the gait profile and the corresponding output voltage.

The impedance matching is useful for load power optimization. Table. 1 shows the impedance of each harvester design at different frequencies. For triboelectric energy harvesters, the average impedance is approximated as $1/(\omega C_{avg})$, (Niu and Wang (2015)), where C_{avg} is the average triboelectric energy harvester inherent capacitance. Increasing the frequency will decrease the impedance. Moreover, any structural parameters that can increase C_{avg} will result in lower impedance. Therefore, an increase in the area size of the triboelectric generator will increase its capacitance and results in lowering its impedance. As deduced from Table. 1, the impedance decreases with the increase of the frequency of the harvester. Also, from Table. 1 we notice a difference in the impedance values for both types of generators which may be due to the difference in the materials used in fabrication. The harvester shape here is a rectangle inside each tibial tray compartment. If the harvester is made such that it closely follows the contour of the tibial tray, it will have a larger area and its impedance will be smaller. However, that will not cause a significant drop. Strategies to improve the efficiency of high impedance devices can be applied to a digitization circuitry to mitigate this problem (Jain et al. (2019)).

	Harvester	
Frequency	**Ti-PDMS-Al**	**Ti-PDMS-Ti**
(Hz)	$\mathbf{R}_o(M\Omega)$	$\mathbf{R}_o(M\Omega)$
1	1050	950
2	366	322
3	200	250

Table 1. Optimal resistance for each triboelectric harvester at different frequencies.

Because of the failure of the rubber springs at full gait loads, we limited the load to 40% of the full gait load so that we can investigate the voltage stabilization of the harvester. In a future study, a full gait load will be used to test the durability once a harder package is designed and fabricated. The testing results for the Ti-PDMS-Al harvester under a different number of cycles for the lateral (L) and medial (M) positions are shown in Fig. 6a. According to Fig. 6a, the harvester shows a monotonic increase in voltage output at both the lateral and medial positions after performing 6k cycles. Even though these variations on the output voltage with varying the number of cycles look small and within a range of $0.5\ V$ in the lateral position, it is still considerable and equivalent to a 25% change. Therefore, for long-term stability, future designs need to be analyzed over a significantly large number of cycles, for example, a million cycle. The information about the variations in the voltage generated can be used to calibrate the digitization circuit. The total nominal force applied during the walking activity will be distributed into two components at the medial and lateral positions, where the medial position will take a larger component than the lateral position (Kumar et al. (2013); Walter et al. (2014)). Our results in Fig. 6a show a possibility to measure the load imbalance in the knee because the harvesters at the medial position generate larger output voltages than the lateral position once the nominal load is the same. To confirm this finding, two identical triboelectric energy harvesters are tested at both the lateral and medial locations under quarter gait load ($500\ N$). The voltage generated from both identical energy harvesters at each location, (Lateral and Medial), is averaged and shown in Fig. 6b. For both harvesters, higher output voltages found to be at the medial location. An indication of a load imbalance can be used to reduce many of the complications after a total knee replacement as the surgeon can take action to fix problems such as misalignment, instability, and excessive wear.

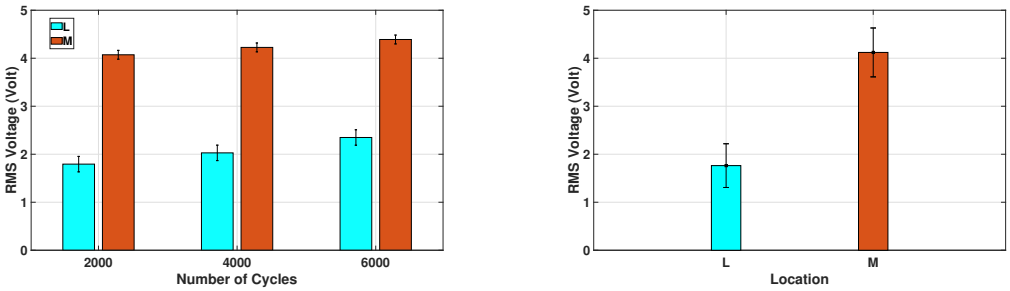

(a) (b)

Figure 6. (a) Long-term voltage outputs of Ti-PDMS-Al at a different number of cycles. Test performed at Quarter gait load and 3 Hz frequency, where M indicates (medial) and L indicates (lateral) portions. The standard deviations and standard error in the Lateral and Medial positions are $(0.16, 0.28)$ and $(0.16, 0.09)$, respectively. (b) Average RMS voltage outputs of Ti-PDMS-Al at the lateral and medial locations for quarter gait load. The standard deviations and standard error in the Lateral and Medial positions are $(0.64, 0.72)$ and $(0.46, 0.51)$, respectively.

The Ti-PDMS-Al was tested for medial location under different input gait loads, where the load was varied to peak values of 200 N, 400 N, 600 N, and 800 N to measure resulting changes in outputs. Fig. 7 shows that higher power and voltage is achieved when higher compressive loads were cyclically applied, although power generation did not scale linearly with the applied load.

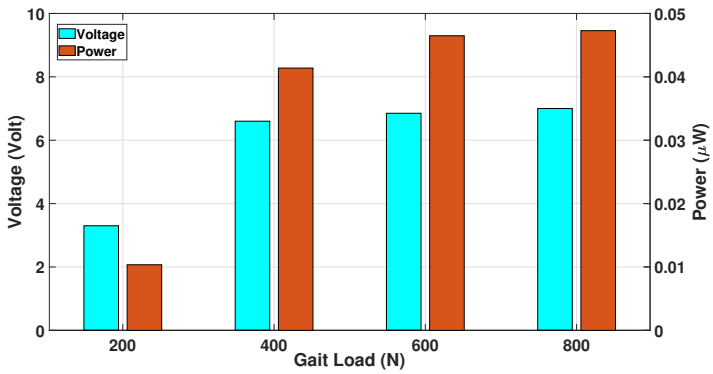

Figure 7. RMS voltage and average power outputs of Ti-PDMS-Al at the medial location for different gait loads.

To evaluate the effect of the material used for the harvester, Ti-PDMS-Al and Ti-PDMS-Ti harvesters are tested under quarter gait load $500\ N$, optimal resistance, and cyclic frequency of 1 Hz at the medial location, and the average output power is measured as depicted in Fig. 8a. While literature is rich in terms of testing Al as the triboelectric material, there is no report on the performance of Ti as the electrode in the triboelectric harvesters. The harvester made mainly of Ti shows higher power output,

which is an interesting finding because Ti is biocompatible material, but Al is not. This selection could help avoid post-surgical complications. The Ti-PDMS-Ti is tested at different frequencies using the resistances mentioned in Table. 1. The resulting power outputs are illustrated in Fig. 8b, where output power is linearly increased with increasing the frequency. The triboelectric generator scavenges power from different ADLs to digitize and store the load data. Inductive coupling (electromagnetic powering) mechanism using a cell phone can be used to transmit the load data wirelessly. In this mechanism, one coil is placed in the implant and one is in an external device such as a cell phone. The power transfers from the cell phone to the implant circuit to read the data. The fact that inductive powering cannot be used to digitize and store the load data is because using continuous inductive powering for measuring and storing causes inconvenience for the user as it requires holding the cell phone close enough to the knee at all times. Since wireless transmission can be done few times a day, inductive powering using a cell phone can easily be done.

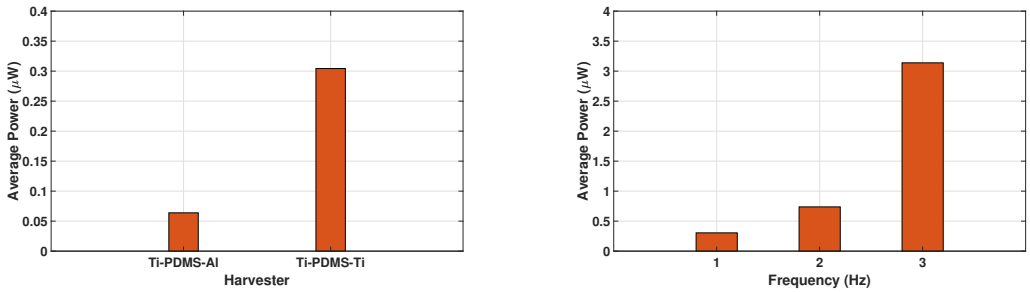

(a) **(b)**

Figure 8. (a) Average power outputs of Ti-PDMS-Al and Ti-PDMS-Ti triboelectric harvesters at medial location under quarter gait load and 1 Hz frequency. (b) Average power outputs of Ti-PDMS-Ti at the medial location as the gait frequency varies.

Parametric Study

Harvester Configuration and Fabrication

To perform this parametric study, the Ti-PDMS-Ti harvester is now sandwiched between two PMMA layers and the two layers are now separated by mechanical springs instead of rubber springs as shown in Fig. 9. The upper layer has dimensions of (30 x 15 x 0.5) mm and is made with sawtooth micro-patterns as shown in Fig. 3b. The lower Titanium layer has similar dimensions to the upper layer and is left to be flat. A PDMS layer is spin-coated on the upper surface of the lower Ti layer.

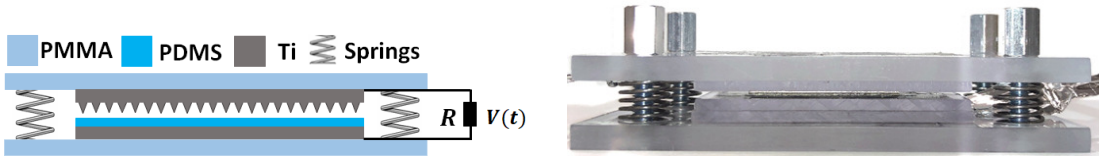

(a) (b)

Figure 9. (a) Schematic of the triboelectric energy harvester configuration, (b) Actual triboelectric energy harvester prototype.

Fabrication of the PDMS layers starts by cleaning the Ti layers with distilled water and acetone using an ultrasonic technique. Then, a PDMS mixture is prepared by adding a 10:1 ratio of silicone elastomer base to a curing agent. After that, the PDMS mixture is vacuumed for an hour to remove air bubbles. Then, the PDMS mixture is spin-coated on the cleaned Ti layers at different RPMs. The Ti layers are then baked at 80^oC for an hour. The thicknesses of the fabricated layers at different RPMs are shown in Table. 2.

To conduct a parametric study of the triboelectric harvester, we use flat PDMS to minimize the effect of random engagement between contacting surfaces. As mentioned above, the PDMS layers were fabricated using a spin coater at specific rpm values to have certain thicknesses along the whole surface of the generator. Making a patterned PDMS layer with a uniform thickness is extremely difficult, and in some spots, there was a chance of short circuit between the top and lower conductor layers. Thus, to obtain robust results and to minimize the effect of random engagement, we have conducted our parametric study on the flat PDMS layer.

RPM	**Thickness** (μm)
500	200
700	140
950	75
1270	65
1690	50
2120	40
2610	25
4500	10

Table 2. The thickness of the fabricated PDMS layers at different RPMs.

Experimental Setup

The experimental setup used to evaluate the performance of the triboelectric harvesters is similar to the setup shown in Fig. 2, with the exception that the AMTI VIVO simulator is replaced with MTS 858 Servo Hydraulic Test System with FlexTest SE Controller. The MTS is responsible for conducting a harmonic axial load, while the amplitude is tuned with the FlexTest controller. The MTS has a built-in load cell to measure the applied force on the harvester. In this test, the axial force profile is assumed to be a half-sine wave signal at 1 Hz. The experimental test is repeated at different external resistances connected to the

harvester to obtain the optimal resistance where maximum power can be achieved. A variable resistance box is used to control the resistance.

Results and Discussion

We conduct the parametric study using a half-sine wave as an extreme case. As mentioned earlier in the discussion of the electrical model of the harvester, represented by Eq. (1), the charge density, $\sigma(t)$, is a function of force that varies with time, thus the voltage variation with the initial gap is not a linear relationship. There will be an optimum value for the initial gap where the voltage will be maximum. The variation of voltage with the thickness t_0 and external resistance R is also nonlinear as Q changes with time. Because of the aforementioned nonlinearity, an empirical approach was used to obtain the optimal PDMS thickness and initial electrode gap and resistance that maximizes the voltage and power output. Fig. 10a shows the pattern of force created by the half-sine wave signal, and Fig. 10b shows the resulting variance of voltage as measured with the electrometer. The resistance used in this test is $1\ M\Omega$ and the applied load has a frequency of $1\ Hz$ with a maximum amplitude of $225\ N$, Fig. 10a. The harvester, under this applied load, generates a maximum peak voltage of $0.3\ V$ as shown in Fig. 10b.

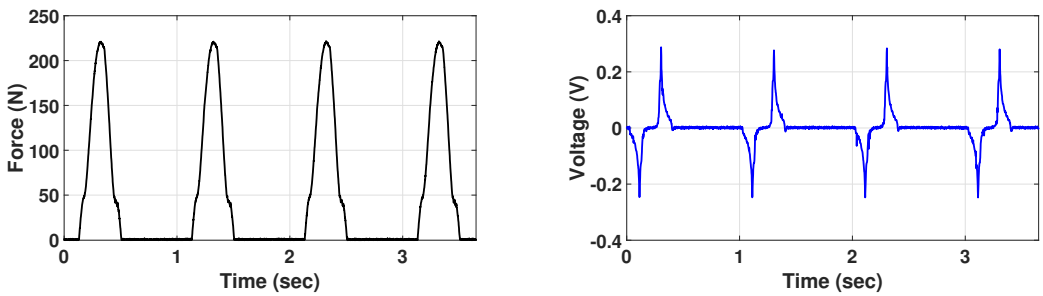

(a) (b)

Figure 10. (a) Load profile for a half-sine-wave load simulated by MTS machine. (b) Generated output voltage.

A zoomed-in and overlapped half-sine-wave load, measured using a built-in load cell in the MTS simulator, and the voltage signal, measured using Keithley electrometer, are shown in Fig. 11. Similar to Fig. 5, both profiles have three distinct regions with respect to the motion of two harvester layers (Ti, PDMS): S: Separation, A: Approaching, C: Contact. The voltage peaks are generated at the Approaching and Separation stages. In this experiment, the zero load amplitude before the approaching stage represents the motion of the MTS upper cylinder from the upper maximum position to the initial contact with the upper electrode of the harvester (Ti). In this region, because of the metallic spring pressing against the top PMMA layer, the distance between the two harvester layers remains constant (Fig. 9). The approaching stage A starts when the MTS cylinder presses against the harvester layers and the load becomes nonzero; the voltage then maximizes in the negative direction and drops until the Ti layer hits the PDMS layer and the contact stage C starts. At the contact stage, when the charges are stabilized, the voltage becomes zero, the pressing load maximizes and drops until the two layers separate, region S. During the separation stage, the voltage maximizes in the opposite direction and then drops to zero. At last, the upper MTS

cylinder disconnects from the harvester, the load drops back to zero and the harvester layers are fully separated. Because of the screws holding the device, the distance between layers remains constant. The nonzero voltage in this region could be because of noise.

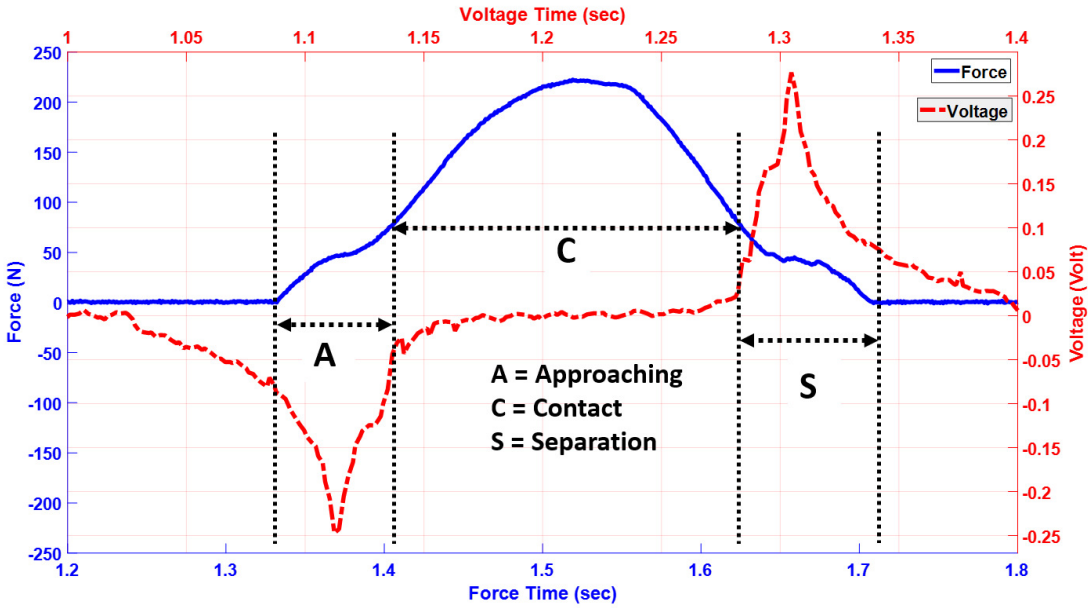

Figure 11. Zoomed-in and overlapped signals of the half-sine force simulated by MTS machine and the corresponding output voltage.

To extract the harvester output power, the internal resistance of the harvester should match the external resistance. To estimate the optimal resistance, the testing was conducted under cyclic compressive load up to 225 N with varied external resistance up to 1 $G\Omega$. Besides, the harvester in this test is built using the lowest layer with PDMS thickness of 200 μm. The variations of the average power outputs with the external resistance load are shown in Fig. 12a. The optimal resistance from the power curve is estimated at 304 $M\Omega$.

To extract the optimal initial gap between the two layers of the triboelectric harvester, the previous harvester is tested under 1 Hz with an input force of 350 N at different gap distances, as shown in Fig. 12b. A similar study of the initial separation effect can be found at Yang et al. (2016). The optimal resistance of 304 $M\Omega$ was used as the external resistance for this test. As the gap distance increases, the average power output rises until it reaches its maximum value at 550 μm. After this distance, the average power output drops rapidly to lower values. The optimum gap distance between the Ti layers is found to be 550 μm (Fig. 12b).

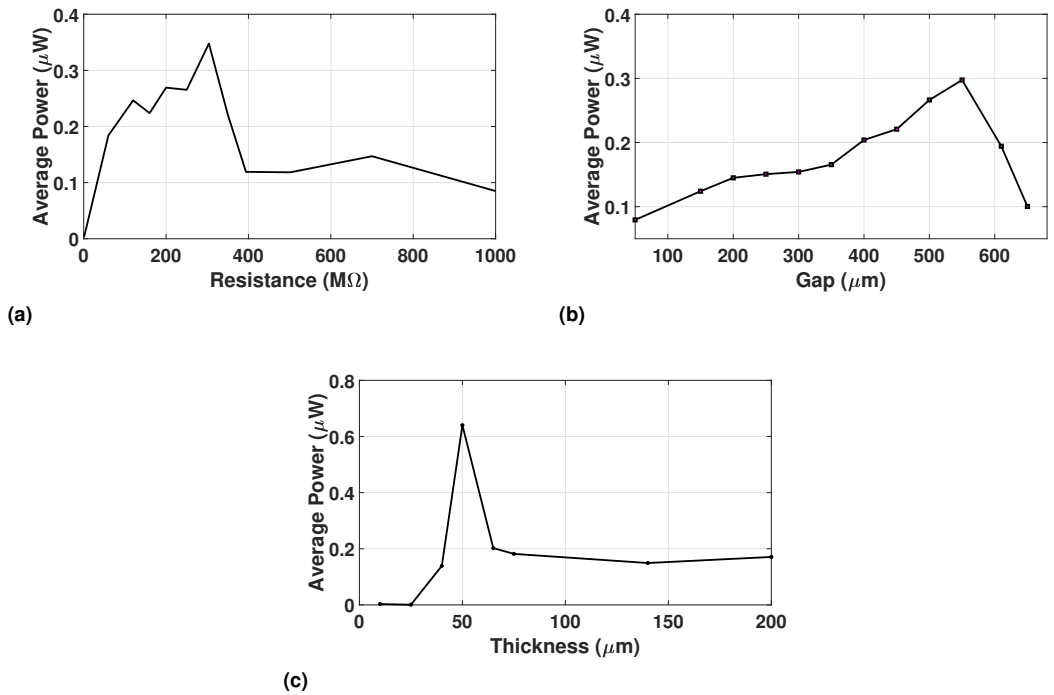

Figure 12. (a) The variation of the average power with external resistance. Optimal resistance found to be $304\ M\Omega$. (b) The variation of the average power with the gap separation distance. Optimal initial gap found to be $550\ \mu m$. (c) The variation of the average power with PDMS thickness. Optimal PDMS thickness found to be $50\mu m$.

Aiming to improve the triboelectric harvester, we examine the influence of the PDMS layer thickness on the output. We tested PDMS layers with thicknesses ranging from $10\ \mu m$ to $200\ \mu m$ while not varying the Ti layers. The voltage and power outputs are measured and the average power is obtained as illustrated in Figure. 12c. For this test, the applied cyclic load is $300\ N$ at $1\ Hz$, while the resistance and initial gap were set at their obtained optimal values. From these graphs, it is possible to observe that average voltage and power outputs increase with an increasing PDMS thickness until reaching a maximum voltage and power values of $14\ V$ and $0.65\ \mu W$ at $50\ \mu m$, respectively.

Proportionality Results:

Results obtained so far were at low loading, while body loads are over $2000\ N$ for average body weight. To investigate the output of the triboelectric harvester at the extracted optimized parameters, the harvester is tested under varying applied forces (Fig. 13). The harvester is made from a lower layer with optimum PDMS thickness ($50\ \mu m$), and optimum gap distance ($550\ \mu m$) connected to optimal resistance ($304\ M\Omega$). Figure. 13 revels the generated voltage and power signal against the axial load. Both results show similar trends, where the generated average voltage and average power increase with increasing the applied cyclic load up to $2300\ N$, where it stabilizes around $23\ V$ and $1.6\ \mu W$, respectively. Compared

to the results in Figure. 12c for the applied force of 300 N, the output power is much less for the same applied force (0.2 μW compared to around 0.6 μW), as shown in Figure. 13b. This difference can be related to the wear that happened to the PDMS layer after the parametric study. The process of making the PDMS including the curing time and temperature has a significant effect on its mechanical properties and durability. It has been reported that ultimate compressive strength decreases with increasing the curing temperature (Johnston et al. (2014)). Closer attention must be made into making a durable PDMS layer, using alternative biocompatible polymer materials such as ethylcellulose and polylactic acid (Sun et al. (2015)), or employing the non-contact mode of harvesting (Wang et al. (2014a)). To estimate the lifetime for in *vivo* implementation, further durability testing on stronger polymer material is needed.

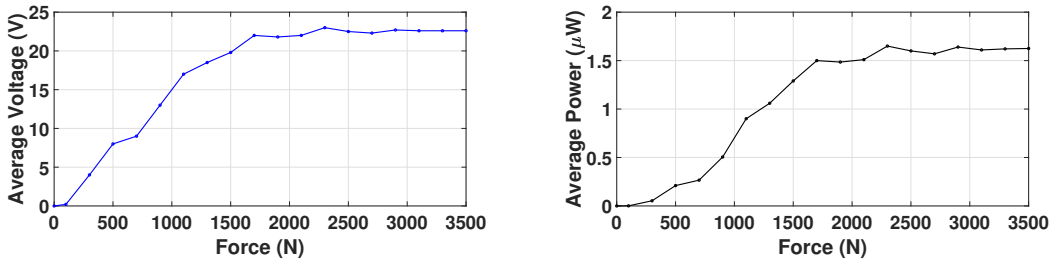

(a) (b)

Figure 13. (a) The variation of the average voltage with applied axial load. (b) The variation of the average power with applied axial load.

Conclusion

The performance of two triboelectric energy harvesters is tested under simulated gait loads using an AMTI VIVO joint motion simulator for the TKR load sensing application. After 6000 cycles, the harvesters in both medial and lateral positions show a monotonic increase in the output power, and future designs need to be analyzed over a significantly large number of cycles. However, this small variation in the output that can be included as part of the digitization circuit calibration. Besides, the harvesters at the medial and lateral positions yield different output, which proves that the triboelectric mechanism can detect load imbalance in the knee. By increasing the load applied, more contact between the harvester layers is created, which results in more power generated. The harvester entirely made of Ti shows higher outputs compared to the harvester made of Ti and Al, which is promising for TKR because of biocompatibility and common use of Ti in orthopedic implants. Furthermore, higher frequencies lead to greater power generation. The titanium harvester was used for the parametric study to optimize the structural parameters of the harvester. For this harvester, we delineate the optimized structural parameters for triboelectric energy harvester to be used in TKR applications. An optimal resistance, optimal gap separation distance, and optimal thickness were extracted to maximize the output average voltage and power. We found the optimal resistance, which is equivalent to the internal resistance, for the triboelectric harvester to be 304 $M\Omega$. The optimal initial gap distance between the triboelectric layers is found to be

$550\ \mu m$, while the optimal thickness for the PDMS layer found to be at $50\ \mu m$. The optimized prototype was tested under different axial loads with a maximum power of $1.6\ \mu m$.

Acknowledgement

Authors are grateful to Dr. Kenneth A. Gall from Duke University for 3D printing Ti layer with micro-patterns.

This research has been supported by the National Institute of Arthritis and Musculoskeletal and Skin Diseases of the National Institute of Health under award number R21AR068572. The content is solely the responsibility of the authors and does not necessarily represent the official views of the National Institute of Health.

References

Almouahed S, Hamitouche C, Stindel E and Roux C (2013) Optimization of an instrumented knee implant prototype according to in-vivo use requirements. In: *Point-of-Care Healthcare Technologies (PHT), 2013 IEEE*. IEEE, pp. 5–8.

Bae J, Lee J, Kim S, Ha J, Lee BS, Park Y, Choong C, Kim JB, Wang ZL, Kim HY et al. (2014) Flutter-driven triboelectrification for harvesting wind energy. *Nature communications* 5: 4929.

Baytekin H, Patashinski A, Branicki M, Baytekin B, Soh S and Grzybowski BA (2011) The mosaic of surface charge in contact electrification. *Science* 333(6040): 308–312.

Bergmann G, Bender A, Graichen F, Dymke J, Rohlmann A, Trepczynski A, Heller MO and Kutzner I (2014) Standardized loads acting in knee implants. *PloS one* 9(1): e86035.

BONNER SM (2007) Tko knee pain with total knee replacement. *Nursing Made Incredibly Easy* 5(2): 30–39.

Burgo TA, Galembeck F and Pollack GH (2016) Where is water in the triboelectric series? *Journal of Electrostatics* 80: 30–33.

Dhakar L, Tay FEH and Lee C (2014) Development of a broadband triboelectric energy harvester with su-8 micropillars. *Journal of Microelectromechanical Systems* 24(1): 91–99.

D'Lima DD, Patil S, Steklov N, Slamin JE and Colwell CW (2006) Tibial forces measured in vivo after total knee arthroplasty. *The Journal of arthroplasty* 21(2): 255–262.

D'Lima DD, Patil S, Steklov N, Chien S and Colwell CW (2007) In vivo knee moments and shear after total knee arthroplasty. *Journal of biomechanics* 40: S11–S17.

D'Lima DD, Townsend CP, Arms SW, Morris BA and Colwell Jr CW (2005) An implantable telemetry device to measure intra-articular tibial forces. *Journal of biomechanics* 38(2): 299–304.

Fan FR, Tian ZQ and Wang ZL (2012) Flexible triboelectric generator. *Nano energy* 1(2): 328–334.

Farhangdoust S, Mehrabi A and Younesian D (2019) Bistable wind-induced vibration energy harvester for self-powered wireless sensors in smart bridge monitoring systems. In: *Nondestructive Characterization and Monitoring of Advanced Materials, Aerospace, Civil Infrastructure, and Transportation XIII*, volume 10971. International Society for Optics and Photonics, p. 109710C.

Gomes A, Rodrigues C, Pereira A and Ventura J (2018) Influence of thickness and contact area on the performance of pdms-based triboelectric nanogenerators. *arXiv preprint arXiv:1803.10070* .

Gooding DM and Kaufman GK (2011) Tribocharging and the triboelectric series. *Encyclopedia of Inorganic and Bioinorganic Chemistry* : 1–9.

Gustke KA, Golladay GJ, Roche MW, Elson LC and Anderson CR (2014) A new method for defining balance: promising short-term clinical outcomes of sensor-guided tka. *The Journal of arthroplasty* 29(5): 955–960.

Han CB, Du W, Zhang C, Tang W, Zhang L and Wang ZL (2014) Harvesting energy from automobile brake in contact and non-contact mode by conjunction of triboelectrication and electrostatic-induction processes. *Nano Energy* 6: 59–65.

Hossain NA, Razavi MJ and Towfighian S (2020) Analysis of mechanical deformation effect on the voltage generation of a vertical contact mode triboelectric generator. *Journal of Micromechanics and Microengineering* 30(4): 045009.

Hu Y, Yang J, Jing Q, Niu S, Wu W and Wang ZL (2013) Triboelectric nanogenerator built on suspended 3d spiral structure as vibration and positioning sensor and wave energy harvester. *ACS nano* 7(11): 10424–10432.

Ibrahim A, Jain M, Salman E, Willing R and Towfighian S (2019) A smart knee implant using triboelectric energy harvesters. *Smart Materials and Structures* 28(2): 025040.

Ibrahim A, Ramini A and Towfighian S (2018) Experimental and theoretical investigation of an impact vibration harvester with triboelectric transduction. *Journal of Sound and Vibration* 416: 111–124.

Jain M, Ibrahim A, Salman E, Stanacevic M, Willing R and Towfighian S (2019) Frontend electronic system for triboelectric harvester in a smart knee implant. In: *2019 IEEE 62nd International Midwest Symposium on Circuits and Systems (MWSCAS)*. IEEE, pp. 386–389.

Jin C, Kia DS, Jones M and Towfighian S (2016) On the contact behavior of micro-/nano-structured interface used in vertical-contact-mode triboelectric nanogenerators. *Nano Energy* 27: 68–77.

Johnston I, McCluskey D, Tan C and Tracey M (2014) Mechanical characterization of bulk sylgard 184 for microfluidics and microengineering. *Journal of Micromechanics and Microengineering* 24(3): 035017.

Kaufman KR, Kovacevic N, Irby SE and Colwell CW (1996) Instrumented implant for measuring tibiofemoral forces. *Journal of biomechanics* 29(5): 667–671.

Ko YH, Nagaraju G, Lee SH and Yu JS (2014) Pdms-based triboelectric and transparent nanogenerators with zno nanorod arrays. *ACS applied materials & interfaces* 6(9): 6631–6637.

Kumar D, Manal KT and Rudolph KS (2013) Knee joint loading during gait in healthy controls and individuals with knee osteoarthritis. *Osteoarthritis and cartilage* 21(2): 298–305.

Kutzner I, Damm P, Heinlein B, Dymke J, Graichen F and Bergmann G (2011) The effect of laterally wedged shoes on the loading of the medial knee compartment-in vivo measurements with instrumented knee implants. *Journal of Orthopaedic Research* 29(12): 1910–1915.

Kutzner I, Heinlein B, Graichen F, Bender A, Rohlmann A, Halder A, Beier A and Bergmann G (2010) Loading of the knee joint during activities of daily living measured in vivo in five subjects. *Journal of biomechanics* 43(11): 2164–2173.

Lin ZH, Cheng G, Wu W, Pradel KC and Wang ZL (2014) Dual-mode triboelectric nanogenerator for harvesting water energy and as a self-powered ethanol nanosensor. *ACS nano* 8(6): 6440–6448.

Lin ZH, Zhu G, Zhou YS, Yang Y, Bai P, Chen J and Wang ZL (2013) A self-powered triboelectric nanosensor for mercury ion detection. *Angewandte Chemie International Edition* 52(19): 5065–5069.

Luciano V, Sardini E, Serpelloni M and Baronio G (2012) Analysis of an electromechanical generator implanted in a human total knee prosthesis. In: *Sensors Applications Symposium (SAS), 2012 IEEE*. IEEE, pp. 1–5.

McCarty LS and Whitesides GM (2008) Electrostatic charging due to separation of ions at interfaces: contact electrification of ionic electrets. *Angewandte Chemie International Edition* 47(12): 2188–2207.

Meneghini RM, Ziemba-Davis MM, Lovro LR, Ireland PH and Damer BM (2016) Can intraoperative sensors determine the "target" ligament balance? early outcomes in total knee arthroplasty. *The Journal of arthroplasty* 31(10): 2181–2187.

Niu S, Liu Y, Zhou YS, Wang S, Lin L and Wang ZL (2015) Optimization of triboelectric nanogenerator charging systems for efficient energy harvesting and storage. *IEEE Transactions on Electron Devices* 62(2): 641–647.

Niu S and Wang ZL (2015) Theoretical systems of triboelectric nanogenerators. *Nano Energy* 14: 161–192.

Ong KL, Lau E, Suggs J, Kurtz SM and Manley MT (2010) Risk of subsequent revision after primary and revision total joint arthroplasty. *Clinical Orthopaedics and Related Research®* 468(11): 3070–3076.

Platt SR, Farritor S, Garvin K and Haider H (2005) The use of piezoelectric ceramics for electric power generation within orthopedic implants. *IEEE/ASME transactions on mechatronics* 10(4): 455–461.

Roche M, Elson L and Anderson C (2014) Dynamic soft tissue balancing in total knee arthroplasty. *Orthopedic Clinics* 45(2): 157–165.

Roundy S, Wright PK and Rabaey J (2003) A study of low level vibrations as a power source for wireless sensor nodes. *Computer communications* 26(11): 1131–1144.

Safaei M, Meneghini RM and Anton SR (2018) Energy harvesting and sensing with embedded piezoelectric ceramics in knee implants. *IEEE/ASME Transactions on Mechatronics* .

Stellbrink C and Trappe HJ (2007) The follow-up of cardiac devices: what to expect for the future? *European Heart Journal Supplements* 9(suppl_I): I113–I115.

Su Y, Wen X, Zhu G, Yang J, Chen J, Bai P, Wu Z, Jiang Y and Wang ZL (2014) Hybrid triboelectric nanogenerator for harvesting water wave energy and as a self-powered distress signal emitter. *Nano Energy* 9: 186–195.

Sun J, Li W, Liu G, Li W and Chen M (2015) Triboelectric nanogenerator based on biocompatible polymer materials. *The Journal of Physical Chemistry C* 119(17): 9061–9068.

Tang W, Tian J, Zheng Q, Yan L, Wang J, Li Z and Wang ZL (2015) Implantable self-powered low-level laser cure system for mouse embryonic osteoblasts' proliferation and differentiation. *ACS nano* 9(8): 7867–7873.

Walter JP, Kinney AL, Banks SA, D'Lima DD, Besier TF, Lloyd DG and Fregly BJ (2014) Muscle synergies may improve optimization prediction of knee contact forces during walking. *Journal of biomechanical engineering* 136(2): 021031.

Wang S, Lin L, Xie Y, Jing Q, Niu S and Wang ZL (2013) Sliding-triboelectric nanogenerators based on in-plane charge-separation mechanism. *Nano letters* 13(5): 2226–2233.

Wang S, Niu S, Yang J, Lin L and Wang ZL (2014a) Quantitative measurements of vibration amplitude using a contact-mode freestanding triboelectric nanogenerator. *ACS nano* 8(12): 12004–12013.

Wang S, Xie Y, Niu S, Lin L and Wang ZL (2014b) Freestanding triboelectric-layer-based nanogenerators for harvesting energy from a moving object or human motion in contact and non-contact modes. *Advanced materials* 26(18): 2818–2824.

Wang ZL (2015) Triboelectric nanogenerators as new energy technology and self-powered sensors–principles, problems and perspectives. *Faraday discussions* 176: 447–458.

Yang B, Zeng W, Peng ZH, Liu SR, Chen K and Tao XM (2016) A fully verified theoretical analysis of contact-mode triboelectric nanogenerators as a wearable power source. *Advanced Energy Materials* 6(16): 1600505.

Yi F, Lin L, Niu S, Yang PK, Wang Z, Chen J, Zhou Y, Zi Y, Wang J, Liao Q et al. (2015) Stretchable-rubber-based triboelectric nanogenerator and its application as self-powered body motion sensors. *Advanced Functional Materials* 25(24): 3688–3696.

Zeng W, Tao XM, Chen S, Shang S, Chan HLW and Choy SH (2013) Highly durable all-fiber nanogenerator for mechanical energy harvesting. *Energy & Environmental Science* 6(9): 2631–2638.

Zhang XS, Han MD, Wang RX, Meng B, Zhu FY, Sun XM, Hu W, Wang W, Li ZH and Zhang HX (2014) High-performance triboelectric nanogenerator with enhanced energy density based on single-step fluorocarbon plasma treatment. *Nano Energy* 4: 123–131.

Zhang XS, Han MD, Wang RX, Zhu FY, Li ZH, Wang W and Zhang HX (2013) Frequency-multiplication high-output triboelectric nanogenerator for sustainably powering biomedical microsystems. *Nano letters* 13(3): 1168–1172.

Zheng Q, Zhang H, Shi B, Xue X, Liu Z, Jin Y, Ma Y, Zou Y, Wang X, An Z et al. (2016) In vivo self-powered wireless cardiac monitoring via implantable triboelectric nanogenerator. *Acs Nano* 10(7): 6510–6518.

Zhou T, Zhang C, Han CB, Fan FR, Tang W and Wang ZL (2014) Woven structured triboelectric nanogenerator for wearable devices. *ACS applied materials & interfaces* 6(16): 14695–14701.

Zhu G, Lin ZH, Jing Q, Bai P, Pan C, Yang Y, Zhou Y and Wang ZL (2013) Toward large-scale energy harvesting by a nanoparticle-enhanced triboelectric nanogenerator. *Nano letters* 13(2): 847–853.

Zhu Y, Yang B, Liu J, Wang X, Wang L, Chen X and Yang C (2016) A flexible and biocompatible triboelectric nanogenerator with tunable internal resistance for powering wearable devices. *Scientific reports* 6: 22233.

Zi Y, Wang J, Wang S, Li S, Wen Z, Guo H and Wang ZL (2016) Effective energy storage from a triboelectric nanogenerator. *Nature communications* 7.